Engle, H. L. James, B. F. Leonard, Eds. (Geological Society of America, Boulder, Colo., 1962), p. 447. However, according to the preliminary results of J. S. Lewis (personal communication), the composition of degassed volatiles could have been the following: H_2O, 20 percent; CO_2, 50 percent; CO, 20 percent; and H_2, 10 percent by volume. This composition is much more reducing than that used in the calculation.

9. M. B. McElroy, *Chemical Processes in the Solar System: A Kinetic Perspective* (Butterworths, London, 1975); Y. L. Yung and M. B. McElroy, *Science* **203**, 1002 (1979). Analyses of the ratio of deuterium to hydrogen by Y. L. Yung and M. B. McElroy [*Bull. Am. Astron. Soc.* **9**, 497 (1977)] and H. Craig and J. E. Lupton [*Earth Planet Sci. Lett.* **31**, 369 (1976)] indicate that large quantitites of H_2 could have escaped from Earth's atmosphere in the past. These results are consistent with an H_2 mixing ratio of $\sim 10^{-3}$ in the primitive atmosphere. The production and subsequent removal of H_2CO represents an additional loss of H_2. However, it is unlikely that such a calculation would yield results outside our current range of estimates for the H_2 mixing ratio.
10. Sources of rate coefficient data are as follows: (a) See Yung and McElroy (*9*). (b) Estimated. A a mean cross section of 3×10^{-19} cm^2 was derived for the visible band from the theoretical study of P. J. Bruna, R. J. Buenker, S. D. Peyerimhoff [*J. Mol. Struct.* **32**, 217 (1976)]. A. A. Borisov, V. T. Galochkin, S. A. Mulenko, A. N. Oraevskii, E. F. Starodubtsev, A. F. Suchkov [*Sov. J. Quantum Electron.* **8**, 1094 (1978)] have estimated mean cross section of 1×10^{-20} cm^2 for the same band. The values of Bruna *et al.* have been used here. (c) J. G. Calvert, J. A. Kerr, K. L. Demerjian, R. D. McQuigg, *Science* **175**, 751 (1972). (d) W. B. DeMore, *Jet Propulsion Lab. Publ. 79-27* (1979). (e) J. A. Logan, M. J. Prather, S. C. Wofsy, *Philos. Trans. R. Soc. London* **290**, 187 (1978). (f) R. T. Watson, personal communication. (g) S. C. Liu and T. M. Donahue, *J. Atmos. Sci.* **31**, 1118 (1974). (h) D. L. Baulch, D. D. Drysdale, J. Duxbury, S. J. Grant, *Evaluated Kinetic Data for High Temperature Reactions* (Butterworths, London, 1976), vol. 3. (i) J. P. Reilly, J. H. Clarke, C. B. Moore, G. C. Pimentel, *J. Chem. Phys.* **69**, 4381 (1978). (j) R. F. Hampson and D. Garvin, Eds., *Reaction Rate and Photochemical Data for Atmospheric Chemistry 1977* (Special Publication 513, National Bureau of Standards, Washington, D.C., 1978). (k) Estimated. (l) W. Hack, H. G. Wagner, K. Hoyermann, *Ber. Bunsenges. Phys. Chem.* **82**, 713 (1978); W. Hack, A. W. Preuss, H. G. Wagner, K. Hoyermann, *ibid.* **83**, 212 (1979).
11. Note that R7 and R8 constitute an effective cycle for the catalytic recombination of atomic hydrogen. This cycle also accounts for the difference in the computed atomic hydrogen densities at low altitudes between this model and that of J. F. Kasting, S. C. Liu, T. M. Donahue, *J. Geophys. Res.* **84**, 3097 (1979).
12. The one-dimensional model extends from 0 to 120 km with a vertical resolution of 2 km, based on the numerical scheme developed by M. Allen, Y. L. Yung, and J. W. Waters (in preparation). The equations of continuity are solved for all species. Vertical transport of long-lived species is described in terms of eddy diffusion. For the standard model, a uniform value of the eddy diffusion coefficient (K) of 10^6 cm^2 sec^{-1} was chosen. Concentrations of the major species H_2O, CO_2, and H_2 were fixed at the lower boundary, and a zero flux was specified for CO. Concentrations of radical species were determined on the basis of their photochemical production and loss rates. A flux of reduced material of $\sim 10^{10}$ cm^{-2} sec^{-1} (mostly as H_2) is required at the lower boundary, in order to maintain the steady state.
13. S. C. Wofsy, *Annu. Rev. Earth Planet. Sci.* **4**, 441 (1976).
14. For H_2 mixing ratios of 10^{-4}, 3×10^{-4}, and 3×10^{-3}, the H_2CO rainout rate is 1.7×10^7, 4.4×10^7, and 1.0×10^9 molecule cm^{-2} sec^{-1}, respectively. For CO_2 mixing ratios of 6×10^{-4}, 1.2×10^{-3}, and 3×10^{-3}, the rainout rate is 4.8×10^8, 1.2×10^9, and 3.1×10^9 cm^{-2} sec^{-1}. Adjusting the value of k_8 to 1×10^{-10}, 2×10^{-10}, and 5×10^{-10} leads to rainout rates of 1.9×10^9, 4.5×10^8, and 1.4×10^8 cm^{-2} sec^{-1}. Adopting a uniform value for K of 10^5 cm^2 sec^{-1} leads to a rainout rate of 2.3×10^8 cm^{-2} sec^{-1}, and raising the surface temperature by 10 percent to 317 K leads to a rainout rate of 8.8×10^7 cm^{-2} sec^{-1}.
15. F. P. Fanale, personal communication.
16. T. Owen, R. D. Cess, V. Ramanathan, *Nature (London)* **277**, 640 (1979).
17. L. Knauth and S. Epstein, *Geochim. Cosmochim. Acta* **40**, 1095 (1976).
18. L. V. Berkner and L. C. Marshall, *J. Atmos. Sci.* **22**, 225 (1965).
19. Perhaps the most important question concerning the fate of H_2CO, once it had been precipitated into the primitive oceans, is its interaction with solar ultraviolet radiation. Preliminary results of G. L. Kok (private communication) indicate that H_2CO in solution does not exhibit the same absorption spectrum as gaseous H_2CO. Photolysis for H_2CO in solution is therefore unlikely, as it undergoes a rapid and almost complete hydrolysis to methylene glycol, $CH_2(OH)_2$, and to other products by processes such as the Cannizzaro reaction [J. F. Walker, *Formaldehyde* (Reinhold, New York, 1964)]. These data imply a certain degree of stability for H_2CO in solution. This question should be investigated further with attention being paid to factors such as pH, the oxidation-reduction state, and the presence of other ultraviolet absorbers in the primitive oceans.
20. C. Ponnamperuma, in *Origin of Prebiological Systems and of Their Molecular Matrices*, S. W. Fox, Ed. (Academic Press, New York, 1965), p. 221.
21. One of us (J.P.P.) thanks J. C. G. Walker for many helpful discussions. We also thank M. Allen, F. P. Fanale, G. L. Kok, C. B. Moore, J. S. Lewis, and J. J. Morgan for their useful comments. J.P.P. is a NASA National Research Council resident research associate. This work was also supported in part by NASA contract NSG-7376 under the Planetary Atmospheres Program. Contribution 3357 of the Division of Geological and Planetary Sciences, California Institute of Technology.

7 February 1980; revised 17 June 1980

Ganymede: A Relationship Between Thermal History and Crater Statistics

Abstract. *An approach for factoring the effects of a planetary thermal history into a predicted set of crater statistics for an icy satellite is developed and forms the basis for subsequent data inversion studies. The key parameter is a thermal evolution–dependent critical time for which craters of a particular size forming earlier do not contribute to present-day statistics. An example is given for the satellite Ganymede and the effect of the thermal history is easily seen in the resulting predicted crater statistics. A preliminary comparison with the data, subject to the uncertainties in ice rheology and impact flux history, suggests a surface age of 3.8 × 10^9 years and a radionuclide abundance of 0.3 times the chondritic value.*

Geomorphic evolution of impact craters on planetary surfaces, created over a wide range of geologic time and a wide spectrum of sizes, provides insight into the temporal behavior of endogenic modification processes. This report presents a simple architecture for generating a set of predicted cumulative impact crater curves reflecting endogenic modification processes on Ganymede. The study was motivated by Voyager spacecraft observations of a relative deficiency of large impact craters (Fig. 1).

A thermal history model is specified and related directly to the viscosity history, the functional forms being fairly well known in terms of flow laws for geologic materials (*1*). The mechanism of crater modification is viscous relaxation, dependent on crater size and the explicit behavior of viscosity with depth. A crater of size D on the surface of Ganymede will have a limited lifetime that depends explicitly on the time of crater formation. This initial model adopts a practical definition of lifetime in terms of a detectability limit based on a critical crater depth, $d_c(D)$. Craters shallower than $d_c(D)$ are not detectable; the specific value of this parameter is an empirical measure from any photograph and is based on resolution, lighting angle, and albedo variation. The lifetime of a crater, $L(t,D)$, is the time differential between creation at time t and the moment when crater depth is less than $d_c(D)$. A critical time $T_0(D)$ is that point in geologic history when $L(t,D)$ extends exactly to the present (*2*).

The predicted cumulative crater statistic, $\hat{\Sigma}(D,t)$, is written as the integral over a differential functional $N(D,t^*)$ such that

$$\hat{\Sigma}(D,t) \equiv \int_D^\infty N(D',t^*)\, dD' \qquad (1)$$

and is the number of craters of size $\geq D$ that exist on a surface formed at time t; the variable t^* is $\max[t,T_0(D)]$. The interpretation of t^* in $N(D,t^*)$ is clear if we envision a surface, formed at time t, that collects craters to the present. We count those craters in the present epoch, but it is clear that by definition if $t < T_0(D)$, craters of size D on the surface formed at t will not last to the present and be counted today. Conversely, if $t > T_0(D)$, craters of size D will persist and be counted.

For a thermal history we assume a scenario starting 4.6×10^9 years ago with a silicate core containing a chronditic complement of radiogenic heat sources, a liquid water mantle, and a surface temperature, T_0, of 100 K. At all times in the history of Ganymede, the Rayleigh number for the mantle is supercritical and convection is the dominant mode of heat transport. The freezing time of the liquid water mantle has been described (*3*). Us-

0036-8075/80/1010-0185$00.50/0

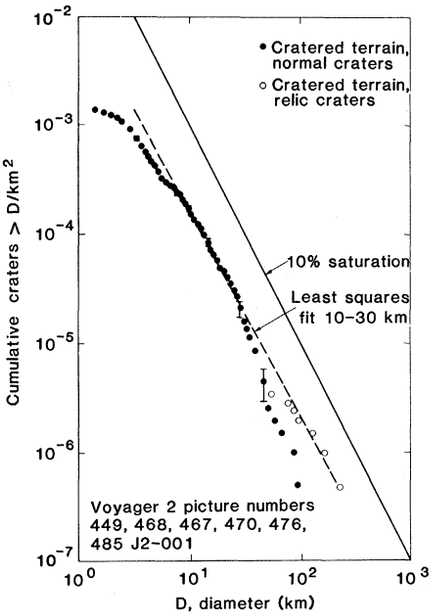

Fig. 1. Cumulative size-frequency curves for normal and relic craters on heavily cratered terrain on Ganymede. The normal crater relationship shows a deficiency of craters larger than ~ 30 km in diameter, which is attributed to viscous degradation of topography due to the material properties of the ice-rich satellite. Relic craters fall close to the projection of the normal crater population, indicated by the least-squares line. Error bars are calculated as $\pm \sqrt{N}$, the cumulative number of craters $\geq D$. An equilibrium population curve at 10 percent saturation is shown for reference.

ing nominal values of the thermal and viscosity parameters (*4*) and the decay characteristics of chondritic sources starting 4.6×10^9 years ago, we obtain a freezing time of about 3×10^8 years.

Subsequent to mantle freezing, heat is transported by subsolidus convection through the mantle to the base of an outer ice shell, or lithosphere, a boundary layer that transports heat conductively to the surface. The thermal evolution is conveniently described by the relationships of parameterized convection (*5*), utilizing the conservation of thermal energy. A solution is obtained for the temperature, T, of an isothermal central region that forms in high-Rayleigh-number convection and for the thickness, Δ, of a thin lithospheric boundary layer at the surface. The results for T and Δ show that at the end of mantle freezing, there is an initial sharp change in both of these variables representing the loss of the remaining primordial heat from the mantle. Subsequently, the mantle is in a steady state, convectively transferring the core heat flux to the surface. With increasing time, however, the values of T decrease and the values of Δ increase, representing the normal decline in radiogenic heat production over the lifetime of the planet. The variables Δ and T completely define the thermal profile necessary to calculate the time-varying viscosity profile for crater relaxation.

A Newtonian viscosity profile is related to the temperature profile as

$$\eta(z,t) = \eta_0 \exp\left\{-a\left[1 - \frac{T_m}{\hat{T}(z,t)}\right]\right\} \quad (2)$$

where z is depth; the temperature profile $\hat{T}(z,t)$ is linear across Δ, varying from T_0 to T, and then of constant value T derived from the parameterized convection solution; the creep constants η_0 and a are from (*3*); and T_m is the melting temperature. The Navier equations for displacement in an elastic medium are decomposed into horizontal wavelengths with Hankel transforms and then solved as differential equations in z. Following McConnell (*6*), the viscosity profile is approximated as a piecewise constant function in z (*7*) and solved by matrix techniques. The elastic equations are changed to viscous equations by the correspondence principle (*8*) and the time dependence thus introduced is solved explicitly by Laplace transform techniques. Since the viscosity profile is a function of time, the problem is solved in successive time stages, with the viscosity profile approximately constant at each stage.

The viscous solution yields displacement at the surface as a function of time; all craters start with unit displacement (depth) and shallow with time. At some point the depth is less than the (normalized) critical depth $\bar{d}_c(D)$ and the crater is assumed to have disappeared from view (*9*)—that is, vanished in terms of morphologic detection (for example, of a rim). Other characteristics may survive and allow the crater to be identified. Relic craters, identified as craterlike albedo features, fall into this class (see Fig. 1 and below).

In Fig. 2 we plot $L(t,D)$ for the nominal thermal model; zero time is 4.6×10^9 years ago. For example, a 60-km crater will survive 10^7 years when formed at 0.6 billion years, but will survive about 10^9 years when formed at 3.0 billion years. The general trend is for increasing lifetimes with decreasing crater size and increasing geologic time. Craters 13 km in diameter or smaller persist from $t = 0$ to the present time t_p (4.6×10^9 years), and for any $t \geq 0$ the trend is for larger craters to persist to the present with increasing time of formation. The exact boundary of the surviving craters is determined graphically by finding the value of t such that $t_p - t = L(t,D)$. This

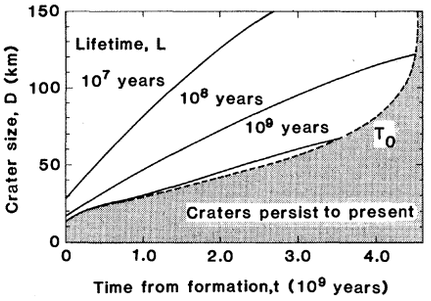

Fig. 2. Crater lifetime $L(t,D)$ for the adopted thermal model (chondritic heat sources in silicate core of Ganymede) is contoured with solid lines. The dashed line bounds the region where craters persist to the present and defines the critical time $T_0(D)$. Craters forming in the white area are not counted in present-day statistics; craters forming in the stippled area are counted.

boundary defines the functional relationship between T_0 and D.

The final element needed to relate our computational model to the observed craters on Ganymede is the temporal relationships for the formation of impact craters. For this simplified model, we have adopted the following relationship as a reasonable cratering flux history; many more complicated models exist. The cumulative number of craters per square kilometer $\geq \Delta$ that have formed since time t is

$$\hat{\Sigma}_i(D,t) = C_i(t)D^{-\alpha} \quad (3)$$

where i denotes the statistics of the flux of impacting objects and differs from the cumulative statistics $\hat{\Sigma}(D,t)$ of the surviving craters on the surface. This is a crater production curve, and the functional relationship between the size and velocity distributions of impacting objects and the size distribution of the craters produced depends on, among other factors, the physical properties of both the impacting object and the target. The variable C_i denotes the time dependence of the flux; the constant α is assumed to be ~ 2 (in more complicated and perhaps more realistic models, α is a function of D). The time-dependent portion of the production model is assumed to consist of a linear contribution that dominates in recent periods and an exponential contribution that dominates in early times

$$C_i(t) = R_p(t_p - t) + Ae^{\lambda(t_p - t)} \quad (4)$$

where R_p is the present production rate of craters, A is the exponential intercept, and λ is the decay constant of the exponential flux (*10*). The time dependence of the survivors on the surface, C, has the same form as C_i but is a function of t^*. However, $\hat{\Sigma}(D,t)$ is not obtained from

$\hat{\Sigma}_i(D,t)$ by replacing $C_i(t)$ with $C(t^*)$ because of the integral nature of Σ (all craters greater than D) and the selectivity of t^* for a specific size. Rather, the differential number of craters of size D is

$$N(D,t^*) = C(t^*)\,\alpha D^{-(\alpha+1)} \quad (5)$$

and $\hat{\Sigma}(D,t)$ is obtained from Eq. 1 by integration. This final step serves, then, to predict crater statistics from a given flux model and thermal history through the critical time $T_0(D)$. Use of this model requires that external modification from other impacts has been minor for the largest crater diameters—this criterion is met on Ganymede.

The crater statistics that result for the specific flux model and two thermal histories are shown in Fig. 3. The solid curves are for chondritic abundances of radiogenics in Ganymede's silicate core. All ages approach a slope of −2 for small D, but these slopes persist to increasing crater size with decreasing age. This indicates that, as Ganymede or any other icy body cools, there is an increase in the size of the largest crater that is unaffected by relaxation processes. The uneven spacing of the curves for equal time increments is a reflection of the competition of the linear and exponential fluxes in the total population, as well as the logarithmic presentation. The dashed curves are for one-tenth chondritic heat sources in the core. It is immediately evident that, for any given age, the size of the largest unaffected crater is increased as the heat source abundance is decreased.

The observed crater relationships (Fig. 1) show two important results. First, the population of normal (nonrelic craters) displays a progressive deficiency of craters larger than about 30 km in diameter, and second, the population of very subdued circular forms (relic craters) follows the trend established by normal craters smaller than 30 km. These results suggest that relic craters evolved from large normal craters, in a manner analogous to that shown in our model.

A comparison of Figs. 1 and 3 leads to an example of the types of interpretation possible with this model. A heat source approximately 0.2 to 0.3 chondritic and a surface age of about 3.8×10^9 years is suggested. However, there are a great many simplifications, uncertainties, and assumptions, and these results must be considered with caution (*11*). The chief uncertainty may be the creep properties of ice at low temperatures. For example, it appears that a viscosity about two orders of magnitude greater allows the chondritic curves to mimic the one-tenth chondritic curves. However, accurate laboratory measurement of low-temperature ice viscosity is within present experimental capability.

We reemphasize that the model used here is preliminary and simplistic and is intended as an illustration of the technique. Our chief point here is that an architecture, the establishment of $T_0(D)$, exists for folding thermal models and flux models into a scheme for predicting crater statistics. Complications (*11*) are details that do not alter the basic approach. The ultimate goal is to use the observed crater statistics to invert for both the thermal and flux histories of the icy satellites. The problem is clearly fraught with ambiguity and one would hope to obtain plausible sets of parameters that reproduce the observations. In that regard, simultaneous inversion of data for different terrain types on Ganymede as well as Callisto data should reduce the level of ambiguity.

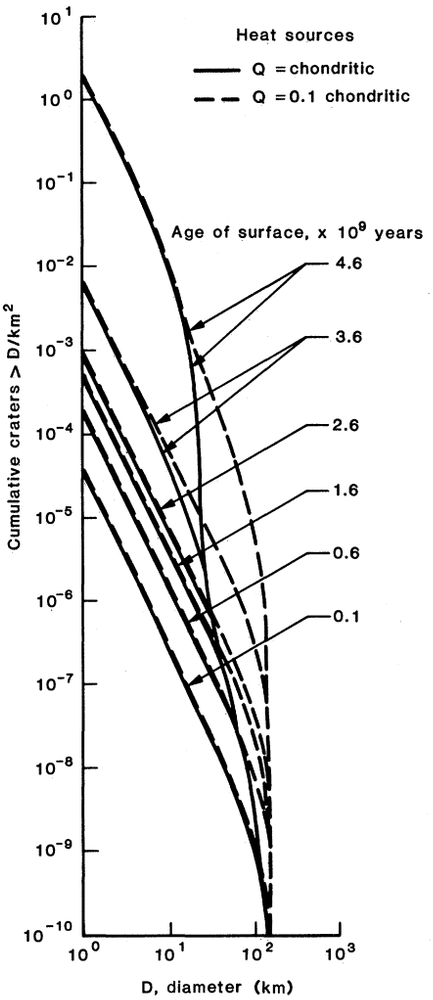

Fig. 3. The crater statistics resulting from $T_0(D)$ of Fig. 2 and the adopted flux model are shown as solid lines. Curves show predicted populations on surfaces of various ages. Dashed curves are the results when the heat source is reduced to a value one-tenth chondritic. On both sets of curves, the slopes approach −2 for small crater diameters, indicating that viscous relaxation processes have not affected these craters.

ROGER J. PHILLIPS
Lunar and Planetary Institute, Houston, Texas 77058

MICHAEL C. MALIN
Department of Geology, Arizona State University, Tempe 85281

References and Notes

1. M. F. Ashby and R. A. Verrall, *Philos. Trans. R. Soc. London Ser. A* **288**, 59 (1978); N. L. Carter, *Rev. Geophys. Space Phys.* **14**, 301 (1976); T. J. Hughes, *J. Glaciol.* **16**, 41 (1976); J. Weertman, in *Physics and Chemistry of Ice*, E. Whalley, S. J. Jones, L. W. Gold, Eds. (Univ. of Toronto Press, Toronto, 1973), p. 320; *Philos. Trans. R. Soc. London Ser. A* **288**, 9 (1978).
2. The variable time t is counted forward from planet formation ($t = 0$). Therefore the present time t_p is $t = 4.6 \times 10^9$ years and age is $t_p - t$.
3. R. T. Reynolds and P. M. Cassen, *Geophys. Res. Lett.* **6**, 121 (1979).
4. The parameters used here are adopted from (*3*). Of particular importance is the parameter a, the diffusion constant for the creep of ice. The value used in this report is $a = 18$. See T. V. Johnson and T. R. McGetchin, *Icarus* **18**, 612 (1973).
5. W. M. Kaula, *J. Geophys. Res.* **84**, 999 (1979); G. Schubert, P. Cassen, R. E. Young, *Icarus* **38**, 192 (1979); H. N. Sharpe and W. R. Peltier, *Geophys. Res. Lett.* **5**, 737 (1978).
6. R. K. McConnell, Jr., *J. Geophys. Res.* **70**, 5171 (1965).
7. The constant vertical increment was successively halved until there was no further change in the answer.
8. D. R. Bland, *The Theory of Linear Viscoelasticity* (Pergamon, New York, 1960).
9. Detection of a crater is, in most cases, dependent on detection of a shadow or shading associated with the crater's wall. For this simplified presentation we have adopted a number of assumptions that allow our results to be compared with the more readily available forms of the Voyager imaging data. (i) Detectability at an average sun elevation angle of 15°, an average resolution of 1 km per pixel, and detection of a 1-pixel shadow results in a threshold depth of 300 m. (ii) A lunarlike depth-to-diameter ratio for fresh craters is adopted as an example, acknowledging that craters formed in ice may have lower d/D ratios (which would tend to make them shallower). Thus 300 m divided by the depth of an equivalent fresh lunar center of diameter D is the fraction below which a crater of diameter D would not be detected = $\bar{d}_c(D)$. (iii) Using a "restored" crater d/D curve [M. C. Malin and D. Dzurisin, *J. Geophys. Res.* **83**, 233 (1978); M. Settle and J. W. Head III, *ibid.* **84**, 3081 (1979)] allows setting an upper limit to crater retention, because the restored curve estimates crater depth as function of diameter prior to wall slumping. Since we assume that all crater changes were viscous rather than brittle, this assumption leads to a calculation of the maximum survivability for a given crater diameter. If the depth were smaller (from slumping or from cratering in less cohesive material, for example) the duration of survival would also be smaller. Our present calculations show, however, that the final set of crater statistics is somewhat insensitive to the exact choice of $\bar{d}_c(D)$.
10. The values used in these calculations are $R_p = 3 \times 10^{-13}$ km^{-2} year^{-1}, $A = 1.8 \times 10^{-12}$ km^{-2}, and $\lambda = 6 \times 10^{-9}$ year^{-1}. These values are nominal lunar parameters and used only for example.
11. We have made a great many simplifications. (i) Ganymede has two distinct terrain types [B. A. Smith *et al.*, *Science* **204**, 951 (1979); *ibid.* **206**, 927 (1979)]; a dark, heavily cratered terrain and a bright, grooved terrain. These two surfaces show different crater densities and morphologies; the grooved terrain shows fewer and fresher looking craters. The relationship of the formation of the grooved terrain to the thermal history must be established or at least parameterized. (ii) Use of models for initial crater depth as a function of diameter and for the critical depth $d_c(D)$, rather than empirical measurements, is

less than optimum. When reliable depth measurements are made and initial crater shapes in icy bodies are better understood, these can be used directly in our procedure. (iii) Convective heat transport has been simplified by the parameterized approach, and the effects of non-Newtonian convection, pressure dependence of melting temperature, and phase boundaries have not been evaluated. We also followed only one evolutionary path, assuming inhomogeneous accretion (or rapid infall of a silicate core) with a primordial liquid mantle. Other paths, such as solid homogeneous accretion of ice and silicates [E. M. Parmentier and J. W. Head, *Proc. 10th Lunar Planet. Sci. Conf.* (1979), p. 2403], may lead to radically different outcomes. The possibility of silicates mixed with ice in the mantle must also be considered in terms of effects on thermal evolution. The effect of non-Newtonian creep on the relaxation of craters must also be considered [E. M. Parmentier and J. W. Head, *J. Geophys. Res.* **84**, 6263 (1979)], as well as the idea that the outer part of the lithosphere should be treated elastically. (iv) There is a similar set of problems associated with any flux model, chief among which is the form of that model. The parameters of the model should be treated as unknown quantities in any inversion process. In addition, the relationship between the velocity and size distribution of the impacting population, the effects of materials on crater geometry, and the production function of craters on the surface must be established, particularly for interplanetary comparisons.

12. We thank E. Abbott, B. Gillette, and M. Williams. This report represents one phase of research carried out at the Jet Propulsion Laboratory, California Institute of Technology, under NASA contract NAS7-100. Lunar and Planetary Institute contribution 413.

1 February 1980; revised 13 June 1980

Hydrogen Release: New Indicator of Fault Activity

Abstract. *The hydrogen concentration in soil gas has been measured in the area around the Yamasaki Fault, one of the active faults in southwestern Japan. Degassing of a significant amount of hydrogen (up to more than 3 percent by volume) has been observed for sites along the fault zone. The hydrogen concentration in soil gas at sites away from the fault zone was about 0.5 part per million, almost the same as that found in the atmosphere. The spatial distribution of sites with high hydrogen concentrations is quite systematic. A hypothesis on the production of hydrogen by fault movements is postulated.*

The upward migration of various gases in the earth's crust is well known. The best known example is the degassing of helium (*1*). It has been suggested that He migrates from the upper mantle because of its anomalous isotopic ratio of ^3He to ^4He (*2*). The degassing rate of He at the surface is thought to be constant except in areas of high crustal activity. Volcanic fumaroles and the degassing observed in geothermal areas are the most extreme cases of this degassing phenomenon.

Degassing rates are assumed to be affected by local geotectonic features such as faulting. A significant amount of He with a high $^3He/^4He$ ratio has been observed along the fault zone formed by the 1966 Matsushiro earthquake swarms (*3*). From these observations, the He flux along the Matsushiro fault was calculated to be about 3×10^4 times (*3*) higher than that of the average crust (*4*).

Recently, the recognition of active faults has become a very important tool for earthquake prediction because many large earthquakes are known to occur along active faults. Several attempts have been made to evaluate the movements of active faults by topographic and geodetic studies and by the observation of microearthquakes. In order to obtain basic knowledge on fault movements by geochemical methods, we have carried out a series of field experiments in the area along the Yamasaki Fault.

This fault is one of the main strike-slip faults in the inner zone of southwestern Japan (*5*). The length of the fault system, trending in a northwest-southeast direction, is about 80 km. The basement rock of the area is primarily Paleozoic granite. The sedimentary layer is less than a few meters thick. Surface features are characterized by altered shales, and a vast amount of Cretaceous intrusives of acidic rocks is seen as rhyolitic dikes (*6*).

Shallow microearthquakes have occurred frequently along the Yamasaki Fault zone. The vertical distribution of the hypocenters of these shocks is concentrated in the region 10 to 15 km deep, the lower part of the granitic layer (*7*). An earthquake with a magnitude of over 4 occurs, on the average, once every several years. Comparatively large earthquakes which occurred recently had magnitudes of 5.1 (21 September 1973), 3.7 (30 September 1977), and 5.0 (28 December 1979). The mean velocity of the left-lateral slip motion of the major fault is calculated to be about 1 mm/year on the basis of neotectonic studies (*8*). Since this area was designated as a test field for earthquake prediction research, intensive studies have been carried out by scientists from several universities in Japan. These include high-sensitivity microseismometry, strainmetry based on continuous observations with an array of extensometers across the fault, leveling, geochemistry, and geomagnetism, among others (*9*).

Since November 1978, field measurements of soil gas have been made three times in the area along the Yamasaki Fault (*10*). A total of 21 sampling sites have been located in the region between Yamasaki and Fukuzaki, an approximate area of 20 km by 20 km (Fig. 1). Each sampling site consists of from 2 to 14 sampling points, so that we could obtain a representative value of the H_2 concentration of that site. A total of 70 sampling points were used in this study.

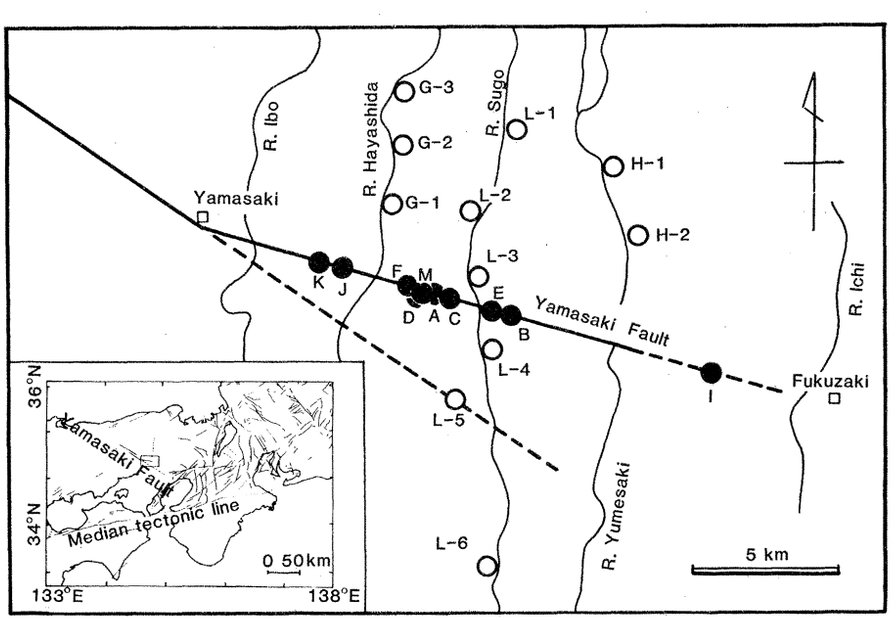

Fig. 1. Locations of the sampling sites of soil gas in the area around the Yamasaki Fault. Representative active faults and tectonic lines in southwestern Japan are shown (*5*). Closed circles indicate the sites where significant amounts of H_2 were measured. Open circles designate the sites where H^2 concentrations were almost the same as that of the atmosphere.

0036-8075/80/1010-0188$00.50/0